# Ta/NiO subwavelength bilayer for wide gamut, strong interference structural color

David Spenato, Matthieu Dubreuil, Denis Morineau, Jean-Philippe Jay, Philippe Giamarchi, David Dekadjevi, Alain Fessant, Sylvain Rivet, Yann Le Grand

# Ta/NiO subwavelength bilayer for wide gamut, strong interference structural color

David Spenato,[1,*] Matthieu Dubreuil,[1] Denis Morineau,[2] Philippe Giamarchi,[1] David Dekadkevi,[1,3] Jean-Philippe Jay,[1] Alain Fessant,[1] Sylvain Rivet,[1] and Yann Le Grand[1]

[1] *Laboratoire d'Optique et de Magnétisme (OPTIMAG), EA 938, IBSAM, Université de Bretagne Occidentale, 29200 Brest, France*

[2] *Institut de Physique de Rennes (IPR), UMR 6251, CNRS, Université de Rennes 1, 35042 Rennes, France*

[3] *Cr Research Group, Department of Physics, University of Johannesburg, PO Box 524, Auckland Park 2006, South Africa*

(Dated: February 18, 2022)

In this paper we demonstrate that Ta/NiO bilayers may be use as high-efficiency, lithography free, reflective structural color filters for generating broad color gamut. Experimental results show that reflectance spectra present deep dips in the visible range, leading to strong structural colors that can be adjusted via the NiO subwavelength layer thickness. Simulation based on thin film interference theory allow to account for the experimental data. We demonstrate that the optical interference effect is still effective when the films are deposited on a flexible substrates such as paper and kapton, enabling to consider flexible color filtering applications.

## I. INTRODUCTION

Selective interaction of light with matter (i.e. wavelength selection) results in colors due to physical processes such as absorption, reflection, refraction, scattering and interference. In a large number of cases, it involves interaction with electrons (i.e. transitions in band structures, orbitals...) [1]. Sometimes it may also arise from geometrical devices such as nano- and microstructures. This is known as "structural color". It produces a selective reflectance of the incident white light according to the nature and organization of the structure. This structural color has been responsible for brighter colors of living animals for million years [2] (i.e. for example the bright and iridescent blue color from Morpho butterfly wings [3]). In the last decades, inspired by the natural living, interaction of light with man-made artificial nano- and micro-structures have been intensively studied [4, 5]. Various technological approaches were used such as plasmon resonance from metal nanostructures, photonic crystals, diffraction from nanostructures arrays, optical resonance of metasurfaces and interference colors in thin films [6–8]. The ability to manipulate light at nano and microscale, has opened in the last decades a huge amount of applications [9] such as color printing [10, 11], solar energy [12], infrared applications, anti reflection and color coating [13, 14]. Conventional, lithography-free, optical anti reflection coatings consist on a single thin film or a stack of thin-films. Light Antireflection (AR) is here based on the principle of destructive interference to supress reflection in the desired wavelenght range according to the film thickness. However these AR coatings are typically of a quarter wavelength thickness ($\lambda$/4n, where n is the refractive index of the material). Recently, novel AR materials using ultra-thin films (with thickness much lower than $\lambda$/4n) have been proposed, consisting of lossy [15] or lossless [16] dielectric films deposited onto non-perfect metallic substrates. Moreover, more complex multilayered structures based on symetrical (i.e metal-insulator-metal) [17] and unsymmetrical Fabry-Perot cavities [18] have been proposed. Despite the rapid development of structural color filters, most nanostructures are rigid once fabricated. In recent years, flexible devices have gained attention due to their potential applications for flexible electronics [9, 19–25].

In this paper we propose and demonstrate high-efficiency, lithography free, reflective structural color filtering for generating wide color gamut. The proposed device structure is based on the low reflectivity metal Ta semi-infinite layer covered with a lossless dielectric nanometer-thick subwavelength NiO layer. NiO was chosen because among all the optical AR coatings involving different materials, NiO is rather overlooked [15, 17, 26–31] and little explored [32] despite the fact that NiO thin films have drawn much attention because their promising potential applications in solar or optoelectronic devices [33–41]. Moreover, because NiO may be considered as a lossless dielectric in the visible range, Ta was chosen because it is a metal with low reflectivity which is mandatory to induce a strong light absorption [16, 32]. Experimental results show that reflectance spectra present deep dips in the visible range, leading to strong structural colors that can be finely and continuously adjusted via the NiO layer thickness. Simulated curves based on thin film interference theory are in good agreement with the experimental curves. We demonstrate that this optical interference effect is still present when the films are deposited on flexible substrates such as paper or kapton.

## II. EXPERIMENTS

Commercially available $Si/SiO_2$ standard Silicon substrates were used to deposit two-layered Ta (50

* david.spenato@univ-brest.fr

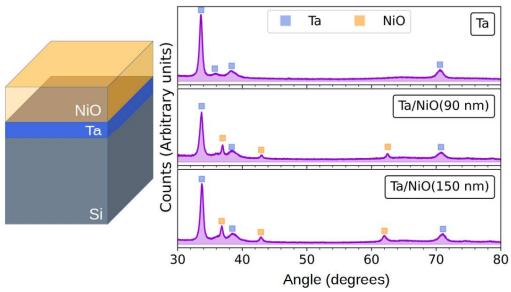


FIG. 1. (a) Schematic drawing of the proposed reflective structural color filter. (b) X-ray diffraction pattern of Si/Ta(50nm), Si/Ta(50nm)/NiO(90nm) and Si/Ta(50nm)/NiO(150nm).

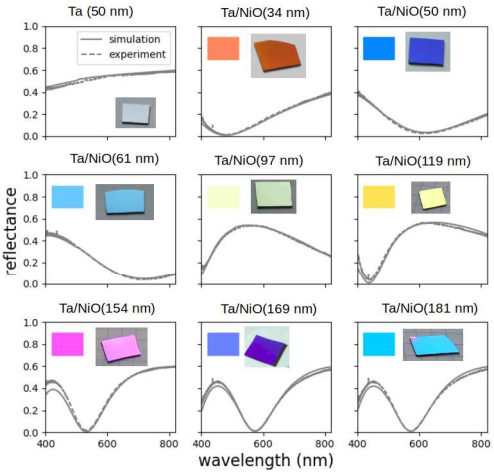


FIG. 2. Experimental and simulated reflectance spectra of the Ta/NiO at 12 degree of incidence for different NiO thicknesses. Inset (left) simulated color (right) photograph of colored samples.

nm)/NiO($t_{NiO}$) structures. The Ta and NiO films where deposited using radio frequency (RF) magnetron sputtering from 3 inches targets. The Ta film was deposited under a power of 100 W and a pressure of $10^{-2}$ mbar. The NiO films were deposited under a power of 50 W and a pressure of $6.10^{-3}$ mbar. With these sputtering conditions the growth rate for the Ta and for the NiO are respectively 0.138 nm/s and 0.0395 nm/s. The nominal NiO thickness were $t_{NiO}$ = 34, 50, 61, 97, 119, 154, 169 and 181nm. Both layers where deposited without substrate heating. A sketch of the stack is presented on Fig.1(a). Structural analysis of the Ta film alone and Ta/NiO films was carried out by X-Ray diffraction (XRD) analysis using CuK radiation $\lambda = 1.54056$ $\AA$ and presented on Fig.1(b). The XRD peaks positions are typical of the one observed on polycristalline Ta [42] and NiO [43, 44] films.

Reflectance spectra were obtained using a collimated light beam from a halogen white light source (Mikropack HL-2000 Ocean Optics), a 12 degree incident angle, and detecting the specular reflection with a 0.6 nm-resolution Vis/NIR spectrometer (SARSPEC, SpecRes+).

The measurements of the refractive indices of Ta and NiO were carried out in the optical region from 300 to 900 nm, at an angle of incidence of 70 degrees, using a Horiba (UVISEL) variable-angle ellipsometer. The measured ellipsometric angles $\Delta$ and $\Psi$ relate respectively to the amplitude ratio and to the phase difference between the complex reflection coefficients according to $r^p/r^s = tan(\Psi)\ e^{i\Delta}$. The results were analyzed with a planar semi-infinite model for Ta and a multilayer model for NiO layers deposited on a Si substrate. The model consistency was verified for four different layer thicknesses.

## III. RESULTS AND DISCUSSION

### A. Reflectance spectra of Ta/NiO bilayers

Fig. 2 displays the experimental unpolarized reflectance spectra for Ta/NiO thin films for nine increasing NiO layer thicknesses (0, 34, 50, 61, 97, 119, 154, 169 and 181 nm).

Clearly the uncoated Ta film has a weak reflectance across the visible spectrum (i.e. it increases from 40 percent to 60 percent). For every NiO thickness, the Ta/NiO bilayers show deep dips in the reflectance spectra. Increasing of the NiO thickness redshifts the resonance dips. It should be noted that for the lowest NiO thicknesses (i.e. 34, 50 and 61 nm) the reflectance spectra shows rather broad resonance compared to larger thickness where the resonance is much sharper. Nevertheless, for the lowest NiO thicknesses a near-zero reflectance is still observed (from 1 to 3.8 percent of reflectance at the dip). Such values are comparable to the one obtained recently on Ni/NiO and Ti/TiO [32]. These sharp dips in the reflectance spectra create a wide variety of interference colors as presented for each NiO/Ta sample on Fig.2.

### B. Simulation of the reflectance spectra

The underlying mechanism for the creation of various colors can be explained in terms of multiple light reflections that occur at the film surface (here NiO) and the interface between the film and the non-perfect metallic substrate (here Ta) as sketched in Fig3. (a) [15, 45]. Complex refractive indices of the film and metallic substrate results in non trivial interface phase shifts , which

can be modified by varying the degree of loss in the film and substrate [13, 15, 16, 46, 47]. Total phase accumulation includes both interface phase shifts and propagation in the film layer. Destructive interferences can thus be obtained at particular wavelengths depending on the sub-wavelength thickness of the film.

Let us consider light incident from air ($N_1$=1) upon a slightly absorbing film (i.e. NiO) with thickness t and complex refractive index $N_2$=$n_2$+i$k_2$ deposited on a metallic semi-infinite substrate with complex refractive index $N_3$=$n_3$+i$k_3$ (i.e. Ta). The equations describing the reflective behavior of incident light on such a three layer structure are given by [13] :

$$r = \frac{r_{12} + r_{23}e^{2i\phi}}{1 + r_{12}r_{23}e^{2i\phi}} \tag{1}$$

where $\phi$=$(2\pi/\lambda)$t$N_2 cos(\theta_2)$ is the complex phase shift accumulated upon wave propagation in the NiO film and $r_{ij}$ are the polarization-dependent Fresnel reflection coefficients for light refracted from medium i to j. These coefficients for s- and p-polarization are given by :

$$r_{ij}^{s} = \frac{N_i \cos(\theta_i) - N_j \cos(\theta_j)}{N_i \cos(\theta_i) + N_j \cos(\theta_j)} \tag{2}$$

$$r_{ij}^{p} = \frac{N_i \cos(\theta_j) - N_j \cos(\theta_i)}{N_i \cos(\theta_j) + N_j \cos(\theta_i)} \tag{3}$$

The angle $\theta_i$ are related to the incidence angle $\theta_1$ by Snell law, $\theta_i$=$\sin^{-1}((N_1/N_i)\sin\theta_1)$. Unpolarized light means an equal amount of power in the s and p polarizations, so that the effective reflectivity of the material is just the average of the two reflectivities :

$$R = \frac{(R^s + R^p)}{2} \text{ with } R^{s,p} = |r^{s,p}|^2 \tag{4}$$

The color of the reflected light is thus determined by the thickness of the NiO layer and the complex refractive indices of NiO and Ta.

The simulated reflectance spectra were generated under Matlab by computing equation (1) and (4) and the results are presented in Fig.2 with the corresponding experimental reflectance spectra. In our simulations, the incident angle $\theta_1$ was set to 12 degrees. For each simulated reflectance spectra the NiO thickess was taken as the nominal deposited thickness. The refractive indices of Ta ($n_3$, $k_3$) and NiO ($n_2$, $k_2$) used for the simulation were those measured by variable-angle spectroscopic ellipsometry experiments that are displayed in Fig.3.

The NiO dispersion curves are fairly flat in the visible range. The extinction coefficient $k_2$ is near zero for $500 < \lambda < 900$ nm and increases rapidly at $\lambda < 400$ nm due to electron interband excitation in the oxyde. Indeed, NiO is a semiconductor with a direct band gap in the range of

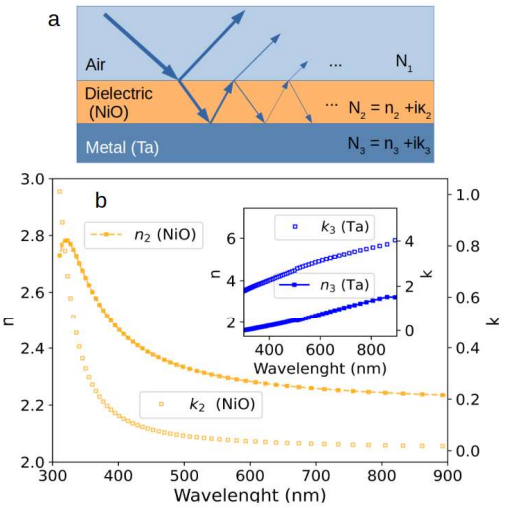


FIG. 3. (a) Schematic diagram of the light propagation in the three layer structure (Air/NiO/Ta) (b) Measured real and imaginary parts of the complex refractive index of NiO ($N_2 = n_2 + ik_2$) and Ta ($N_3 = n_3 + ik_3$)(*inset*) obtained by spectroscopic ellipsometry.

3.0-4.0 eV as usually observed for sputtered nickel oxyde thin films [48]. The refractive index is between 2.46 and 2.24 in the visible region. Both NiO refractive index ($n_2$) and extinction coefficient ($k_2$) dispersion curves are typical of NiO thin films [40, 49]. For tantalum, the refractive indices $n_3$ and $k_3$ respectively monotonously increase from 1.63 and 1.85 to 3.22 and 4.03 for $300 < \lambda < 900$ nm.

It should be noted that because NiO is a lossless dielectric in the visible range, light absorption principally occurs inside the metallic substrate [16]

Fig.2 compares the simulated reflective spectra (solid lines) to the experimental ones (dashed lines) and presents a good agreement between experiments and numerical predictions.

### C. Color gamut

Each reflection spectra was transformed into CIE chromaticy coordinates x and y and was further converted to to sRGB values for display (detailed explanation for converting spectra to colors maybe found in several textbook [50] or papers [51]). Simulated sRGB colors deduced from the simulated reflectance spectra are presented in Fig.2 and turn out to be in good accordance with the observed colors. In order to illustrate the variety of colors of our proposed structure, and to explore the color gamut, we have simulated color change in a wide range of NiO thicknesses. The results are presented in Fig.4. Clearly a rich color palette may be obtained with NiO/Ta bilayers by varying the NiO thickness.

Flexible structural colors attract extensive interest ow-

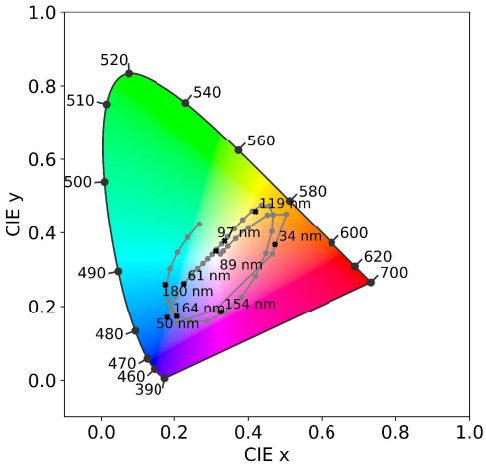


FIG. 4. Grey dots: Simulated color gamut maped in the CIE chromaticy diamgram, representing the range of color variation when the thickness of the NiO layer is change from 5 to 200 nm in steps of 5 nm. Black dots : Chromaticity coordinates of the measured reflectance spectra of our Ta/NiO samples.

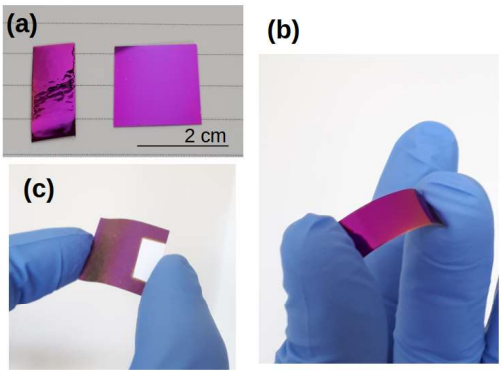


FIG. 5. Photographs of the Ta/NiO(154nm) sputtered on (a) Kapton (left) Glass (right) (c) paper. (b) A gloved hand bending the sample sputtered on Kapton

ing to their potential optolectronic applications. We have thus sputtered the NiO/Ta bilayers onto different flexible substrates: commercial Kapton®and commercial drawing paper. The flexible structural colored samples with different colors adhere perfectly onto these substrates. Fig. 5 shows typical photographs for these flexible samples bent or not.

Because they are much thinner than the wavelength of light, ultrathin coatings have a low sensitivity to the angle of incidence. Indeed, with most of such coatings, the absorption features remain prominent for angle of incidence from 0 to 60 degrees as observed for lossy [15] or lossless dielectrics [16]

Due to the low angular sensitivity enabled by the sub-wavelength NiO layer thickness, the property of the flexible structural color remains almost unchanged when the colored membranes are bent. Furthermore, the fabrication technique of the flexible version of our color system is compatible with current micro-/nanofabrication industrial methods and has potential for large-scale production.

## IV. CONCLUSION

In this paper we have demonstrated that Ta/NiO bilayers may be use as high-efficiency, lithography free, reflective structural color filters for generating broad color gamut. Experimental results show that reflectance spectra present deep dips in the visible leading to strong structural colors that can be adjust via the NiO layer sub-wavelength thickness. Simulated curves based on thin film interference effect well account for the measured reflectivity spectra. Moreover we have shown that this optical interference effect is still present when the films are deposited on flexible substrates such as paper an kapton which makes these nanostructures widely applicable, and may be used for flexible color filtering devices.

## REFERENCES

[1] K. Nassau, The fifteen causes of color: The physics and chemistry of color, Color Research & Application **12**, 4 (1987).
[2] A. R. Parker, 515 million years of structural colour, Journal of Optics A: Pure and Applied Optics **2**, R15 (2000).
[3] S. Zhang and Y. Chen, Nanofabrication and coloration study of artificial morpho butterfly wings with aligned lamellae layers, Scientific Reports **5**, 1 (2015).
[4] Y. Zhao, Z. Xie, H. Gu, C. Zhu, and Z. Gu, Bio-inspired variable structural color materials, Chem. Soc. Rev. **41**, 3297 (2012).
[5] L. Shang, W. Zhang, K. Xu, and Y. Zhao, Bio-inspired intelligent structural color materials, Mater. Horiz. **6**, 945 (2019).
[6] A. Kristensen, J. K. W. Yang, S. I. Bozhevolnyi, S. Link, P. Nordlander, N. J. Halas, and N. A. Mortensen, Plasmonic colour generation, Nature Reviews Materials **2**, 16088 (2017).
[7] A. Shaukat, F. Noble, and K. M. Arif, Nanostructured color filters: A review of recent developments, Nanomaterials **10**, 10.3390/nano10081554 (2020).

[8] C. Ji, K.-T. Lee, T. Xu, J. Zhou, H. J. Park, and L. J. Guo, Engineering light at the nanoscale: Structural color filters and broadband perfect absorbers, Advanced Optical Materials **5**, 1700368 (2017).

[9] Z. Xuan, J. Li, Q. Liu, F. Yi, S. Wang, and W. Lu, Artificial structural colors and applications, The Innovation **2**, 100081 (2021).

[10] A. V. Yakovlev, V. A. Milichko, V. V. Vinogradov, and A. V. Vinogradov, Inkjet Color Printing by Interference Nanostructures, ACS Nano **10**, 3078 (2016).

[11] F. Cheng, J. Gao, T. S. Luk, and X. Yang, Structural color printing based on plasmonic metasurfaces of perfect light absorption, Scientific Reports **5**, 11045 (2015).

[12] H. J. Park, T. Xu, J. Y. Lee, A. Ledbetter, and L. J. Guo, Photonic Color Filters Integrated with Organic Solar Cells for Energy Harvesting, ACS Nano **5**, 7055 (2011).

[13] M. A. Kats and F. Capasso, Optical absorbers based on strong interference in ultra-thin films, Laser & Photonics Reviews **10**, 735 (2016).

[14] W. Fan, J. Zeng, Q. Gan, D. Ji, H. Song, W. Liu, L. Shi, and L. Wu, Iridescence-controlled and flexibly tunable retroreflective structural color film for smart displays, Science Advances **5**, 10.1126/sciadv.aaw8755 (2019).

[15] M. A. Kats, R. Blanchard, P. Genevet, and F. Capasso, Nanometre optical coatings based on strong interference effects in highly absorbing media, Nature Materials **12**, 20 (2013).

[16] M. ElKabbash, S. Iram, T. Letsou, M. Hinczewski, and G. Strangi, Designer perfect light absorption using ultrathin lossless dielectrics on absorptive substrates, Advanced Optical Materials **6**, 1800672 (2018).

[17] Z. Li, S. Butun, and K. Aydin, Large-Area, Lithography-Free Super Absorbers and Color Filters at Visible Frequencies Using Ultrathin Metallic Films, ACS Photonics **2**, 183 (2015).

[18] C. Yang, W. Shen, Y. Zhang, K. Li, X. Fang, X. Zhang, and X. Liu, Compact multilayer film structure for angle insensitive color filtering, Scientific Reports **5**, 9285 (2015).

[19] M. A. Kats and F. Capasso, Ultra-thin optical interference coatings on rough and flexible substrates, Applied Physics Letters **105**, 131108 (2014).

[20] C.-S. Park and S.-S. Lee, Narrowband and flexible perfect absorber based on a thin-film nano-resonator incorporating a dielectric overlay, Scientific Reports **10**, 17727 (2020).

[21] Y. Su, X. Tang, G. Huang, and P. Zhang, Large-area, flexible, full-color printings based on asymmetry fabryperot cavity resonances, Optics Communications **464**, 125483 (2020).

[22] Z.-J. Zhao, M. Lee, H. Kang, S. Hwang, S. Jeon, N. Park, S.-H. Park, and J.-H. Jeong, Eight inch wafer-scale flexible polarization-dependent color filters with ag–tio2 composite nanowires, ACS Applied Materials & Interfaces **10**, 9188 (2018).

[23] K.-T. Lee, S. Y. Han, Z. Li, H. W. Baac, and H. J. Park, Flexible high-color-purity structural color filters based on a higher-order optical resonance suppression, Scientific Reports **9**, 14917 (2019).

[24] J. Zhao, M. Qiu, X. Yu, X. Yang, W. Jin, D. Lei, and Y. Yu, Defining deep-subwavelength-resolution, wide-color-gamut, and large-viewing-angle flexible subtractive colors with an ultrathin asymmetric fabryperot lossy cavity, Advanced Optical Materials **7**, 1900646 (2019).

[25] F. Chen, S.-W. Wang, X. Liu, R. Ji, L. Yu, X. Chen, and W. Lu, High performance colored selective absorbers for architecturally integrated solar applications, J. Mater. Chem. A **3**, 7353 (2015).

[26] C. Yang, W. Shen, Y. Zhang, K. Li, X. Fang, X. Zhang, and X. Liu, Compact Multilayer Film Structure for Angle Insensitive Color Filtering, Scientific Reports **5**, 9285 (2015).

[27] Z. Wang, X. Wang, S. Cong, J. Chen, H. Sun, Z. Chen, G. Song, F. Geng, Q. Chen, and Z. Zhao, Towards full-colour tunability of inorganic electrochromic devices using ultracompact fabry-perot nanocavities, Nature Communications **11**, 302 (2020).

[28] S. J. Kim, S. Kim, J. Lee, Y. Jo, Y.-S. Seo, M. Lee, Y. Lee, C. R. Cho, J.-p. Kim, M. Cheon, J. Hwang, Y. I. Kim, Y.-H. Kim, Y.-M. Kim, A. Soon, M. Choi, W. S. Choi, S.-Y. Jeong, and Y. H. Lee, Color of copper/copper oxide, Advanced Materials **33**, 2007345 (2021).

[29] Z. Yang, C. Ji, D. Liu, and L. J. Guo, Enhancing the purity of reflective structural colors with ultrathin bilayer media as effective ideal absorbers, Advanced Optical Materials **7**, 1900739 (2019).

[30] A. S. Rana, M. Zubair, M. S. Anwar, M. Saleem, and M. Q. Mehmood, Engineering the absorption spectra of thin film multilayer absorbers for enhanced color purity in cmy color filters, Opt. Mater. Express **10**, 268 (2020).

[31] J. Tan, Z. Wu, K. Xu, Y. Meng, G. Jin, L. Wang, and Y. Wang, Numerical study of an au-zno-al perfect absorber for a color filter with a high quality factor, Plasmonics **15**, 293 (2020).

[32] T. Letsou, M. ElKabbash, S. Iram, M. Hinczewski, and G. Strangi, Heat-induced perfect light absorption in thin-film metasurfaces for structural coloring, Opt. Mater. Express **9**, 1386 (2019).

[33] M. Taeo, D. Maestre, and A. Cremades, An approach to emerging optical and optoelectronic applications based on nio micro- and nanostructures, Nanophotonics **10**, 1785 (2021).

[34] B. Mistry, P. Bhatt, K. Bhavsar, S. Trivedi, U. Trivedi, and U. Joshi, Growth and properties of transparent p-NiO/n-ITO (In2o3:Sn) pn junction thin film diode, Thin Solid Films **519**, 3840 (2011).

[35] C.-T. Lee, C.-C. Chen, and H.-Y. Lee, Three dimensional-stacked complementary thin-film transistors using n-type Al:ZnO and p-type NiO thin-film transistors, Scientific Reports **8**, 3968 (2018).

[36] P. Qin, M. Linder, T. Brinck, G. Boschloo, A. Hagfeldt, and L. Sun, High Incident Photon-to-Current Conversion Efficiency of p-Type Dye-Sensitized Solar Cells Based on NiO and Organic Chromophores, Advanced Materials **21**, 2993 (2009).

[37] H. Lee, Y.-T. Huang, M. W. Horn, and S.-P. Feng, Engineered optical and electrical performance of rfsputtered undoped nickel oxide thin films for inverted perovskite solar cells, Scientific Reports **8**, 10.1038/s41598-018-23907-0 (2018).

[38] D. Di Girolamo, F. Di Giacomo, F. Matteocci, A. G. Marrani, D. Dini, and A. Abate, Progress, highlights and perspectives on nio in perovskite photovoltaics, Chemical Science **11**, 7746 (2020).

[39] R. A. Wahyuono, B. Seidler, S. Bold, A. Dellith, J. Dellith, J. Ahner, P. Wintergerst, G. Lowe, M. D. Hager, M. Wächtler, C. Streb, U. S. Schubert, S. Rau, and B. Dietzek, Photocathodes beyond nio: charge transfer dy-

namics in a $\pi$-conjugated polymer functionalized with ru photosensitizers, Scientific Reports **11**, 2787 (2021).

[40] K. Sun, F. H. Saadi, M. F. Lichterman, W. G. Hale, H.-P. Wang, X. Zhou, N. T. Plymale, S. T. Omelchenko, J.-H. He, K. M. Papadantonakis, B. S. Brunschwig, and N. S. Lewis, Stable solar-driven oxidation of water by semiconducting photoanodes protected by transparent catalytic nickel oxide films, Proceedings of the National Academy of Sciences of the United States of America **112**, 3612 (2015), 25762067[pmid].

[41] K. Sun, M. T. McDowell, A. C. Nielander, S. Hu, M. R. Shaner, F. Yang, B. S. Brunschwig, and N. S. Lewis, Stable solar-driven water oxidation to o2(g) by nioxide-coated silicon photoanodes, The Journal of Physical Chemistry Letters **6**, 592 (2015).

[42] A. Navid and A. Hodge, Nanostructured alpha and beta tantalum formationrelationship between plasma parameters and microstructure, Materials Science and Engineering: A **536**, 49 (2012).

[43] H.-L. Chen, Y.-M. Lu, and W.-S. Hwang, Thickness dependence of electrical and optical properties of sputtered nickel oxide films, Thin Solid Films **514**, 361 (2006).

[44] D. T. Dekadjevi, A. Suvorova, S. Pogossian, D. Spenato, and J. Ben Youssef, Experimental evidence for the role of nonuniform modes in the asymmetric magnetization reversal of a NiNiO system, Phys. Rev. B **74**, 100402 (2006).

[45] H. Pan, Z. Wen, Z. Tang, G. Xu, X. Pan, Q. Xu, Y. Lu, H. Xu, Y. Sun, N. Dai, and J. Hao, Wide gamut, angle-insensitive structural colors based on deep-subwavelength bilayer media, Nanophotonics **9**, 3385 (2020).

[46] J. Rensberg, Y. Zhou, S. Richter, C. Wan, S. Zhang, P. Schöppe, R. Schmidt-Grund, S. Ramanathan, F. Capasso, M. Kats, and C. Ronning, Epsilon-near-zero substrate engineering for ultrathin-film perfect absorbers, Physical review applied **8**, 014009 (2017).

[47] N. Yu and F. Capasso, Flat optics with designer metasurfaces, Nature Materials **13**, 139 (2014).

[48] K. S. Usha, R. Sivakumar, and C. Sanjeeviraja, Optical constants and dispersion energy parameters of nio thin films prepared by radio frequency magnetron sputtering technique, Journal of Applied Physics **114**, 123501 (2013).

[49] A. Al-Ghamdi, W. E. Mahmoud, S. Yaghmour, and F. Al-Marzouki, Structure and optical properties of nanocrystalline nio thin film synthesized by solgel spin-coating method, Journal of Alloys and Compounds **486**, 9 (2009).

[50] Colorimetry: Understanding the cie system, (2007).

[51] Y. Chen, J. Mandal, W. Li, A. Smith-Washington, C.-C. Tsai, W. Huang, S. Shrestha, N. Yu, R. P. S. Han, A. Cao, and Y. Yang, Colored and paintable bilayer coatings with high solar-infrared reflectance for efficient cooling, Science Advances **6** (2020).